A method for quantifying the time of cooling in thermochronometric inversions

Kalin T. McDannell[1] and C. Brenhin Keller[1]

[1]Department of Earth Sciences, Dartmouth College, Hanover, New Hampshire, USA

Correspondence: Kalin McDannell (kalin.t.mcdannell@dartmouth.edu)

Abstract. Reconstructing geological processes and events from thermochronometric data typically requires the interpretation of time-temperature path ensembles calculated by inverse methods. Commonly, this may be as simple as associating heating or cooling in thermal histories with specific geologic events and indirectly "dating" such events by estimating the time of observed heating or cooling. While visual assessments may suffice in the simplest cases, statistical comparison requires quan-
5 titative estimations of the time of cooling. This study presents a straightforward methodology wherein we ascertain the time of peak cooling for the entire cooling signal within a thermal history model. The focus is on the time-temperature paths intersecting the half-maximum cooling isotherm, where the full distribution of interpolated model times at that isotherm provides a quantitative metric for the characteristic "time of cooling". We apply this method to thermochronologic inversions of synthetic and natural examples, demonstrating its practicality and functionality. This systematic approach provides an effective means
10 of quantitatively reporting the peak cooling time from thermal history inversions.

1 Introduction

The ability to discern information about both time and temperature makes thermochronology a particularly useful tool for understanding geological processes such as mountain building, sedimentary basin formation, and landscape evolution (Reiners et al., 2017). Methodological standards and analytical capabilities have progressed significantly since the inception of modern
15 thermochronology in the 1970s, improving data quantity and quality. At the same time, data modelling and interpretation have advanced due in part to increased computational resources. The power and limitations of such data, i.e., radiation damage-diffusivity relationships and kinetic model calibration, respectively, have been an ongoing focus of discussion and research (e.g., Gautheron and Zeitler, 2020; Guenthner, 2021). However, inverse models still represent one of the most fundamental ways we interpret thermochronometric dates by predicting thermal histories that best explain those data.

20 Historically, the simplest class of study involves connecting individually constrained time-temperature (t–T) points between individual mineral dates, often in the context of plutonic cooling, uplift, and exhumation (e.g., Mattinson, 1978; Harrison et al., 1979). However, interpreting thermochronometric cooling ages and relating them to surface processes and crustal geodynamics has been a major focus of work over the last few decades (e.g., Stüwe et al., 1994; House et al., 1998; Ehlers and Farley, 2003; Braun, 2005; Kohn et al., 2005; Reiners and Brandon, 2006; Braun et al., 2012; Fox et al., 2014a). Typically in more
25 recent applications, sophisticated numerical modeling programs execute a stochastic search of t–T space for plausible thermal

histories that reproduce input thermochronological data (e.g., Gallagher, 1995; Issler, 1996a; Willett, 1997; Ketcham, 2005; Gallagher, 2012; Keller et al., 2022).

Even with modern techniques and models, the examination of thermal histories in geologic context frequently raises a simple question: when did cooling occur? Despite the ubiquity of this interpretive framing, a systematic approach to defining
30 and quantifying the time of cooling within inversions has to our knowledge never been thoroughly discussed in the literature. The specific times of model cooling (or heating) are typically associated with past geological events of interest, making it increasingly critical to establish statistical methods that allow for the quantification and quantitative comparison of such heating and cooling events. The ad hoc method most often used is a visual estimate—where cooling initiation is typically framed with respect to a specific temperature at the time of maximum reheating preceding cooling—in other words, the point where there is
35 a change from heating to cooling. The turning point[1] is identified for a single representative t–T path (e.g., best fit to the data) and an approximate cooling time is reported. A commonly encountered statement about the timing of cooling may be directly associated with the sensitivity of a thermochronometer, for example, "based on apatite fission-track data, cooling from ~ 110 °C began ca. 70 Ma", or in some cases, even more general descriptions are provided, "cooling occurred in the Late Cretaceous" or "between approximately 80–70 Ma". Such descriptions are probably sufficient for simple histories or for inverse models
40 based on a single thermochronometer where degrees of freedom are purposefully minimized (e.g., Green and Duddy, 2012). Depending on the geologic problem, however, more specific or quantitative estimates may be necessary.

A few questions remain unanswered, specifically, (i) is the conventional t–T path turning point the best way to determine the timing of cooling and does that truly represent the maximal cooling peak, (ii) what uncertainties or biases may influence cooling time determination, and (iii) is there a more systematic metric by which we can formalize cooling time estimates?

45 ## 2 Considerations for thermal history models

Before addressing these questions, it is useful to review some of the commonly applied medium-to-low temperature thermochronological methods and their temperature sensitivities. The following thermochronometers provide constraints across temperatures encountered in the upper crust (Reiners et al., 2017, for review), including, potassium feldspar ^{40}Ar/^{39}Ar ($\sim$
350–150 °C), zircon fission track ($\sim$ 260–200 °C), zircon (U–Th)/He (ZHe; $\sim$ 180–30 °C), apatite fission track (AFT; $\sim$
50 140–50 °C), apatite (U–Th)/He (AHe; $\sim$ 90–40 °C), and apatite ^{4}He/^{3}He dating ($\sim$ 50–35 °C). Each of the aforementioned methods is a powerful tool for understanding crustal evolution, although, many studies typically incorporate no more than one or two techniques for logistical and practical reasons. However, applying a single method limits what we can infer about a geological history through modeling, thus requiring careful consideration of the various factors that affect quantifying the timing of cooling within inverse thermal history models and how to best deal with them.

---

[1]Often (though inaccurately) referred to as the "inflection point." Here we use *turning point* to denote the point where the first derivative (slope) of a curve changes sign, indicating a change in the direction of the curve, i.e., a local maximum or minimum where the derivative equals 0. *Inflection point* is the point on a curve where the second derivative (curvature) changes sign.
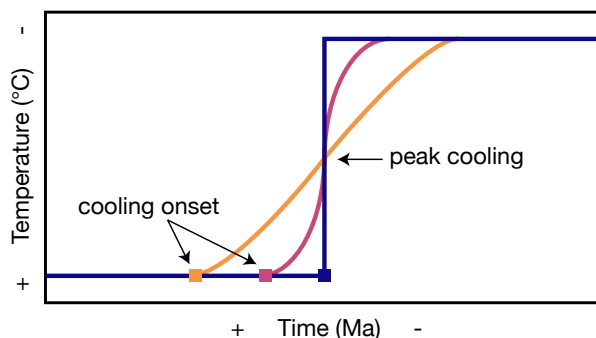
Figure 1. Schematic time-temperature plot showing three cooling curves from high to low temperature with different cooling rates. The time of maximum or peak cooling, when the first derivative of the cooling curve is maximized, is the same for all *t*–*T* paths shown here, whereas cooling onset is different for each path (except for the instantaneous cooling step function). Peak cooling is the true inflection point of the *t*–*T* path. In practice, the time of cooling onset is conditional on the resolving power of thermochronometer data with respect to the total cooling signal (i.e., on how well the model prediction matches the real thermal history).

2.1 Geologic setting and cooling rate

Cooling rate is a subtle albeit consequential feature that varies with other parameters within inversions (e.g., mineral grain size or radiation damage effects; Whipp et al., 2022) and is difficult to quantify a priori. There are many aspects of determining rates that are specific to inversion code (i.e., randomization, *t*–*T* node discretization, interpolation, etc.) that are beyond the scope of this paper, but we simply point out basic rate-related features that affect model results and interpretation.

It is well established that rock cooling rates are inherently related to geodynamic environment—active mountain belts experience relatively faster cooling than stable cratons due to the effects of and interactions between tectonic uplift, surface processes, relief generation, and mass/heat advection (e.g., Reiners and Brandon, 2006). Thermal history models for active settings will naturally differ from relatively inactive geological settings. With respect to inversion behavior, rapid cooling scenarios may manifest nearly identical (i.e., synchronous) times for cooling initiation, heating-to-cooling turning points, and thermochronometric sensitivity onset within a model (Figure 1); therefore, estimating the peak timing of cooling is potentially more straightforward. Such behavior may be expected in active tectonic settings with relatively simple histories dominated by only monotonic cooling—such as areas of the Himalaya where apparent cooling ages are usually young (< 1–10 Ma) for high- and low-temperature thermochronometers spanning > 300 °C due to rapid uplift (e.g., Herman et al., 2010; Zeitler et al., 2014). Active settings have been the primary focus of most thermochronology research over the past few decades, so it is perhaps unsurprising that estimating the cooling time in models was never discussed in much detail. Conversely, regions that have experienced slow or episodic heating/cooling may require a more quantitative and consistent assessment of the peak cooling time within a thermal history model.

2.2 Thermochronometer resolution

Here we are primarily concerned with cooling paths in $t–T$ models. In most situations, thermochronometer resolving power is
75   dependent upon the magnitude of the relevant cooling event and whether the specific thermochronometer(s) applied can fully
resolve an associated $t–T$ cooling history within the uncertainty limits of a particular method (e.g., kinetic model uncertainty
or parent-daughter isotopic heterogeneity; Fox and Shuster, 2014; Fox et al., 2017). Cooling onset is frequently the focus of
attention in the published literature—but the time at which cooling "begins" in a model is very sensitive to uncertainty in
the $t–T$ paths—analogous to how the minimum age of a population is sensitive to the uncertainty of the geochronometer (e.g.,
80   Vermeesch, 2021). Therefore, the "onset of cooling" for a thermal history is an unreliable metric because it is highly influenced
by the sensitivity of the chronometer data (i.e., how well the model $t–T$ path matches some real cooling signal). The frequency
and magnitude of reheating episodes that may ensue after initial cooling may further complicate signal fidelity.

2.3 Imposed model constraints

An underappreciated bias that may have unintended consequences on modeling outcomes is the influence of imposed con-
85   straints on cooling path vertices and inflections. Time and temperature are correlated—a change in time or temperature at
any point along a single model path can be compensated by another change along that path (i.e., individual $t–T$ points are
conditional on the other parts of the history; Willett, 1997; Fox and Carter, 2020; Gallagher, 2023). Therefore, any fixed or
purposefully limited point along a path can have far-reaching consequences on model behavior that may not be entirely obvi-
ous. If constraints are of high quality and have a physical basis, such treatment is required and beneficial, but often constraints
90   based on physical geology and those based on assumed conditions or interpretations are given equal model weighting, which
is highly problematic because alternate hypotheses are ignored and uncertainties underestimated (McDannell et al., 2022b).
These effects are compounded for certain circumstances. For example, the influence of imposed constraints on other parts of
the thermal history inevitably increases as thermochronometer resolving power decreases, therefore, $t–T$ path vertices outside
of "constraint boxes" may be indirectly controlled by enforced constraint placement rather than chronometric data if $t–T$ sen-
95   sitivity is poor (Vermeesch and Tian, 2014; McDannell and Issler, 2021; McDannell et al., 2022b). A practical way to mitigate
this issue is to use multiple chronometers with a range of $t–T$ sensitivities, only apply indisputable geological constraints, and
to specify exactly the time and associated temperature range over which cooling is being constrained and interpreted within a
model and how that may relate to any superposed constraints.

3 Quantifying peak cooling time

100 The information required to estimate the cooling time is inherently linked to thermochronometric sensitivity, the thermal history
that a rock experienced, and our ability to recover that history with inverse methods. The interaction of and trade-offs between
various parameters in models can affect such estimates, including but not limited to: heating and cooling rates, diffusion and
annealing kinetic [model] uncertainties (e.g., Carlson et al., 1999; Shuster et al., 2006; Stephenson et al., 2006; Gautheron et al.,

2009; Willett et al., 2017; Ginster et al., 2019; Guenthner, 2021), analytical conditions and statistical treatment of data (e.g.,
105 Galbraith, 2005; Ketcham et al., 2009, 2018; Vermeesch, 2019; McDannell, 2020; Flowers et al., 2023), geological constraints
and their associated uncertainty (e.g., McDannell and Issler, 2021; McDannell et al., 2022b), and the application of one or
multiple thermochronometers (e.g., Fox and Shuster, 2020; McDannell and Flowers, 2020). As discussed previously, many of
these sources of uncertainty are the focus of ongoing work, whereas the effects of others can be minimized with careful sample
and data treatment or addressed in quantitative ways (i.e., Bayesian resampling of kinetic or data uncertainties) rather than be
110 entirely overlooked.

3.1 Full time-Distribution at Half-Maximum temperature (FDHM)

Here we consider a statistical technique to address some of the aforementioned issues by focusing on the distribution of the
time of cooling through a characteristic isotherm, allowing us to quantify both the mean or median and uncertainty of this
distribution. That is, in the context of an inversion, we focus on the times at which the accepted model cooling paths pass
115 through an isotherm representing the midpoint of a particular cooling event. The half-maximum isotherm of the total cooling
is identified within a time window in the thermochronological inversion, that is, the midpoint of the cooling event, which
conveniently also represents the time of fastest cooling, as well as the inflection point (point of change in sign of second
derivative) in the case of a smooth symmetrical cooling curve with a single inflection point. The half-maximum isotherm is
preferred because the cooling path centroid is the true inflection point where the sign of curvature or concavity changes in a
120 smooth thermal history progressing from high to low temperature (Fig. 1). Our name for this distribution at the half-maximum
isotherm was chosen in the spirit of the spectroscopic term "full width at half-maximum" (FWHM), which is the distance
between points on a curve (or distribution) at half of the maximum amplitude— a simple measure of the width of a distribution
(Markevich and Gertner, 1989). Here we consider a full distribution rather than merely a width, so the adopted nomenclature
is "full distribution at half-maximum" (FDHM) for this interpolated time distribution at the half-maximum temperature.
125   This procedure was first applied in McDannell and Keller (2022) and the Julia source code is documented on the GitHub or-
ganization *OpenThermochronology* (https://github.com/OpenThermochronology/CoolingFDHM), which is a communal open-
source code repository for thermochronological tools and time-temperature inversion software. Currently, the FDHM code is
specific to QTQt model output (Gallagher, 2012), but could be modified to accept $t–T$ paths from other modeling software.
    The FDHM is not only a method to quantify peak cooling but is also an indirect measure of $t–T$ resolution, since the first
130 derivative of a cooling curve represents the temporal distribution for when cooling occurred in a model (within an interval of
interest). To quantify this, first, the time at which each thermal history solution passes through the half-maximum isotherm
is recorded and those data are then linearly interpolated within a time window and plotted as a histogram. The peak of the
distribution (i.e., mode) is selected and values at half of the peak represent the full distribution, or the FDHM. The time
window, time interpolation step, and the histogram bin size (all in units of Myr) are variables that may require tuning based on
135 the timescale of the specific problem under investigation.
    One assumption involved with the FDHM calculation is that a complete cooling signal is being captured fully by the model.
If that assumption is invalid—either when the total magnitude of cooling is unknown/highly uncertain, or if a single reset

thermochronometer is modeled, one can only accurately estimate instead the time at which sensitivity begins for the specific thermochronometer(s) being inverted in the model (e.g., 120 °C isotherm for AFT). The "total annealing temperature" is a

140   similar concept that has long been utilized for the AFT method but is infrequently reported in the published literature. Beyond the definition pertaining to the temperature of total erasure of a fission-track population subjected to linear heating, the total annealing temperature is an estimate of sensitivity based on the formation of the oldest [remaining] track during an episode of cooling—and indirectly equates to the track "retention age"—the time(s) at which the oldest track(s) form (and survive until present day) for a suite of model thermal histories (Issler, 1996b; Willett, 1997; Ketcham et al., 1999). This also ideologically

145   parallels the "closure temperature" for Fickian diffusion in minerals (Dodson, 1973), which represents the temperature when half of the radiogenic isotope yield is retained in a crystal for a monotonic cooling path (Gautheron and Zeitler, 2020). All of these metrics (similar to "cooling onset") become more difficult to interpret when t–T paths depart from rapid monotonic cooling.

3.2 Testing the FDHM method using synthetic data

150   We tested the FDHM approach by initially forward modeling simple cooling-only thermal histories spanning 1200 Myr and 200 °C of total cooling. The time span of each history is less important than the style and cooling trajectory, and the exercises shown in this section with synthetic data are focused on using straightforward scenarios rather than consider all the nuances of thermal history inversion.

We examined a step-like history where cooling from 240 °C to 40 °C occurs roughly halfway through a >1 Gyr record—

155   similar to some cases recently much debated in the literature. Thermal histories were forward modelled in QTQt v. 5.8.0 (Gallagher, 2012) and cooling rates of 10 °C Myr^{-1} and 1 °C Myr^{-1} were arbitrarily assessed (Figure 2). Synthetic thermochronometer data were predicted for the ZHe, AFT, and AHe systems from the aforementioned histories (Table 1). One difference is that rather than being entirely isothermal prior to cooling (i.e., Figure 1), the t–T path begins at 300 °C at 1200 Ma and cools first through apparent closure of the ZHe chronometer.

160   Eight synthetic ZHe grains were modelled with the radiation damage diffusivity kinetics of Guenthner et al. (2013). Zircons span a broad range of U values (Th and Sm neglected for simplicity) of 50–2000 ppm and grain sizes were fixed at 40 μm spherical radius to better exploit the relationship between ZHe date and radiation damage (i.e., effective uranium, eU = [U] + 0.238*[Th] + 0.0012*[Sm]; radiation damage proxy). Three AHe dates were generated using the Flowers et al. (2009) kinetic model with U values of 10, 25, and 50 ppm and spherical radii of 75, 60, and 40 μm, respectively. The synthetic AFT samples

165   were modeled in QTQt (Table 1) using the multikinetic annealing model of Ketcham et al. (2007) set to typical fluorapatite annealing kinetics (r_{mr0} = 0.83). The r_{mr0} is a fitted parameter defining the relationship between the reduced track length of a more annealing resistant apatite at the t–T conditions where a less resistant apatite first becomes totally annealed (Carlson et al., 1999; Ketcham et al., 1999). For comparison, an r_{mr0} of 0.83 is equivalent to a measured Cl value of 0.0 atoms per formula unit (apfu), or a Dpar value of $\sim$ 1.77 μm within the revised kinetic scheme of Ketcham et al. (2007). Refer to McDannell

170   and Issler (2021) and Issler et al. (2022) for a recent discussion of the r_{mr0} kinetic parameter in relation to thermal history resolution and sensitivity.

Table 1. Predicted synthetic thermochronometer data

	10 °C Myr^{-1}		**1 °C Myr^{-1}**		
	Date	**±**	**Date**	**±**	**eU**
ZHe	498.6	10.9	494.1	10.4	50
	499.4	14.9	500.9	14.5	100
	500.5	12.0	509.6	12.2	250
	501.3	13.0	515.1	13.3	500
	501.7	11.0	517.3	11.4	750
	501.9	8.0	518.1	8.3	1000
	502.2	9.0	516.9	9.3	1500
	494.6	5.8	480.2	5.6	2000
AHe	532.6	13.9	475.9	12.4	10
	443.6	8.9	393.8	7.8	25
	527.7	9.5	473.7	8.5	50
AFT	643.1	17.1	597.6	15.8	–
MTL	14.5	0.8	14.4	0.9	–

(U-Th)/He dates are not corrected for α-ejection (i.e., no Ft correction) and total uncertainties are randomly assigned up to 3% of the cooling age. Here, eU = U, where contributions from Th and Sm are ignored. AFT age is the central age $\pm\,1\sigma$ (n = 40). MTL = c-axis projected mean track length; number of lengths is 150 for all examples, 5.5 M etchant.

3.3 Synthetic data inversion and FDHM results

The synthetic data were inverted in an attempt to recover each forward modeled thermal history in QTQt. The general prior in QTQt was set to 600 ± 600 Myr and 150 ± 150 °C with a fixed modern surface temperature of 20 °C and an essentially unconstrained maximum allowable heating/cooling rate ($\delta T/\delta t$) of 1000 °C Myr^{-1}. To better facilitate recovery of the true path, reheating was prevented in the inversions, age uncertainties were minimized (Table 1), and a starting t–T point was pinned to 1200 ± 1 Ma at 300 ± 1 °C. The QTQt temperature step for diffusion was set to 3 (AHe) and 6 (ZHe), while the radiation damage step was set to 2 (AHe) and 4 (ZHe). In addition, the option in QTQt to "reject more complex models that do not improve data fit" was not implemented since this explicit penalty is not a formal Bayesian Markov Chain Monte Carlo (MCMC) procedure and we were interested in examining the full suite of accepted histories.

The inversions were completed with a short burn-in of 150,000 iterations that were discarded, followed by 250,000 iterations that were retained post burn-in to assess the posterior distribution of accepted thermal histories. A primary purpose of the MCMC burn-in phase is exploration of the full model space, thus the parts of the model domain shown here with zero
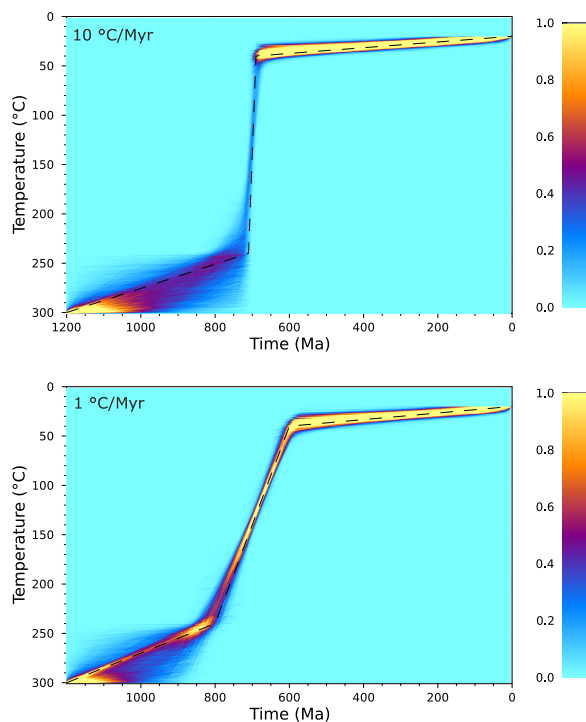
Figure 2. QTQt inversions of synthetic ZHe, AFT, and AHe data predicted from histories characterized by 10 °C Myr^{-1} and 1 °C Myr^{-1} cooling rates. The half-maximum isotherm is 140 °C at 700 Ma (see text for details). Models are shown as a heat map of path density resolved to a pixel size of 1 Myr and 1 °C. Relative probability is proportional to path density, where brighter colors and higher saturation indicate more thermal histories pass through that region of t–T space. Color scale is the normalized path density, where a minimum value of 0 is equal to no paths, and a maximum value of 1 is equal to the upper 95th percentile of path density. The dashed black line is the true thermal history being recovered. All synthetic input data were reproduced within uncertainty by the model. Burn-in iterations: 150,000; post burn-in iterations: 250,000. In this case, the agreement between the "true" history and the model t–T paths (i.e., between observed and predicted data) demonstrate convergence to a stable posterior distribution.

path density (cyan color; Figure 2) does not imply that those regions of t–T space were not searched, which is a common

185   misconception. Fewer total iterations are required to reach model convergence because our inversions utilize synthetic data implicitly assuming ideal kinetic models without additional sources of uncertainty. Actual thermal history models integrated across thermochronometric systems and large datasets typically require burn-in (and post burn-in) on the order of $\gg 10^5$ to 10^6 iterations to yield well sampled, stable posterior t–T path distributions (e.g., McDannell et al., 2022a; McDannell and Keller, 2022). The latter point is critical for obtaining reliable model results for natural samples with presumably complex histories, especially in deep time.

190
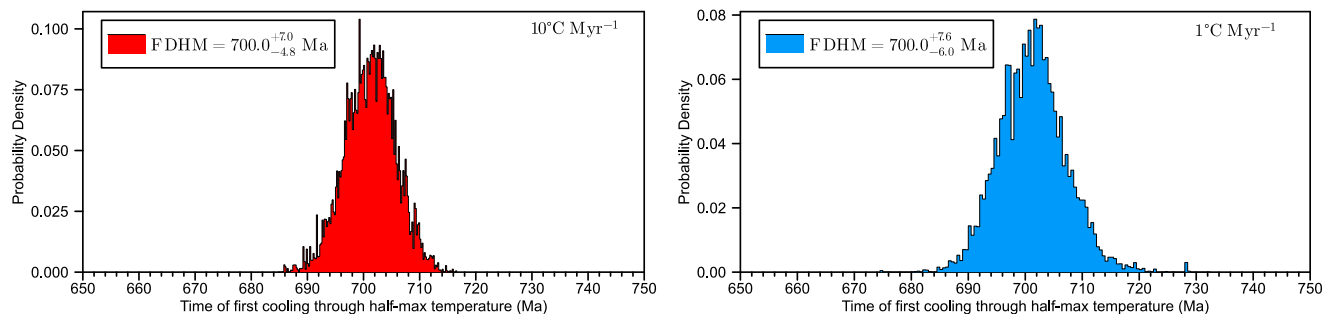
Figure 3. Probability density plots of the times when thermal histories crossed the 140 °C isotherm, or half maximum of total cooling between 240 and 40 °C for the 10 °C Myr^{-1} and 1 °C Myr^{-1} cooling rate models shown in Figure 2. The time of peak cooling for the true path is 700 Ma in both examples. The time window examined for each model was between 750–650 Myr and linear interpolation step was 0.1 Myr for the temporal distributions with a histogram bin size of 4 Myr. FDHM = full distribution at half maximum.

The QTQt inversions successfully recovered the thermal history that was used to generate the synthetic data (Figure 2). A total 200 °C of cooling occurs between 710 Ma and 690 Ma (10 °C Myr^{-1}) and between 800 Ma and 600 Ma (1 °C Myr^{-1}) for the true history being recovered and also passes through the half-maximum isotherm at 700 Ma. The FDHM was then calculated at the 140 °C isotherm (Figure 3) because that is half of the total cooling between 240–40 °C in each history from Figure 2, with the only distinction between each model being the interval over which cooling occurs as a function of

195   cooling rate. A key feature of the inversions is that the total cooling magnitude was accurately recovered. The time of peak cooling in the QTQt models from the FDHM method is 700.0 $^{+7.0}_{-4.8}$ Ma (10 °C Myr^{-1}) and 700.0 $^{+7.6}_{-6.0}$ Ma (1 °C Myr^{-1}) for each respective inversion, which confirms that the FDHM method can recover the true half-maximum, or peak cooling, with a modest level of uncertainty in this case (Figure 3). Improved time-temperature resolution was a result of the integrated ZHe,

200   AFT, and AHe data. The fact that the synthetic data also had small uncertainties resulted in well resolved thermal histories, which then propagated into the FDHM estimate. Thus, if the data uncertainties increase, then the uncertainty in the thermal histories and FDHM also increase. This was verified with other synthetic data inversions that are not shown here for the sake of brevity.

3.4   Synthetic data inversion: Apatite (U-Th)/He only

205   Inversions of thermochronometric mineral systems are increasingly interpreted, either individually or in a combined fashion, across longer timescales where model results require careful interpretation. The application of multiple thermochronometers with bracketing or redundant information can better constrain complex thermal histories compared to any one chronometer alone (e.g., McDannell et al., 2019; McDannell and Flowers, 2020; McDannell and Issler, 2021). To constrain the peak timing of cooling using low-temperature thermochronometers, the total cooling magnitude must be equivalent to the temperature

210   sensitivity of the method—otherwise only a portion of a longer cooling path will be accurately recorded (McDannell and
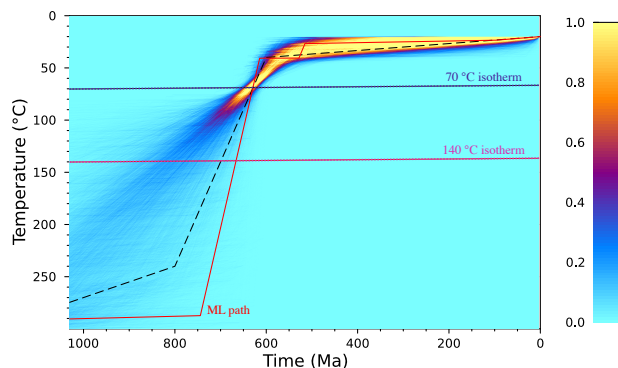
Figure 4. QTQt model for the 1 °C Myr^{-1} cooling rate history. Only apatite (U-Th)/He data were inverted. The dashed black path is the true thermal history being recovered and the red curve is the Maximum Likelihood (ML) path, or best fit to the data. Refer to Figure 5 for FDHMs.

Keller, 2022, for discussion). For example, if the total cooling magnitude is 200 °C, and a thermochronometer is only sensitive to temperatures $\leq$ 70 °C, then the apparent cooling onset in the model will be temporally biased by the difference in time between the true cooling onset and data sensitivity onset, in proportion to the slope of the cooling curve (i.e., cooling rate). In such a situation, cooling onset and maximum/peak cooling would only be the same for near instantaneous cooling (Figure 1),

215 and would be progressively different for slower cooling scenarios.

Our first simulations maximized t–T sensitivity by utilizing all of the data from the ZHe, AFT, and AHe thermochronometers. Now we show a second model where only the synthetic AHe data were inverted. The second simulation was carried out to assess the hypothesized model behavior with respect to partial resolution of a longer cooling segment. We kept all other QTQt conditions the same as previously discussed except for the pinned inversion start at 300 °C at 1200 Ma. The removal of the

220 high-temperature constraint averted an overly simplistic t–T path dominating the accepted posterior histories (due to lower resolution from only a single thermochronometer).

The AHe-only inversion is shown for the 1 °C Myr^{-1} cooling history (Figure 4). The highest relative likelihood is apparent from the highest path density in QTQt, which clearly occurs below 100 °C and the true thermal history is only accurately recovered below ca. 50 °C. As previously mentioned, the true time of peak cooling is 700 Ma at the 140 °C isotherm, whereas

225 the FDHM for that isotherm in the AHe-only inversion is 778.0 $^{+67.0}_{-106.9}$ Ma (Figure 5a). The FDHM result is highy uncertain and an inaccurate overestimate of the actual peak cooling time, minimizing the utility of the metric, since reporting peak cooling between ca. 845–671 Ma is not very informative if utilized for geologic interpretation.

Models that inadequately resolve the true peak cooling time, or those where the total cooling magnitude is highly uncertain, should be carefully interpreted. To aid in this effort we take advantage of QTQt output. The "closure time" (i.e., tc in default

230 QTQt plots, *HeClosureTime* in output file) is an approximation of when He retention begins and is an estimate of how far back in time the history is constrained by each apatite. The apparent "closure ages" for the AHe dates derived from the true 1 °C

GEOCHRONOLOGY
Discussions
EGU
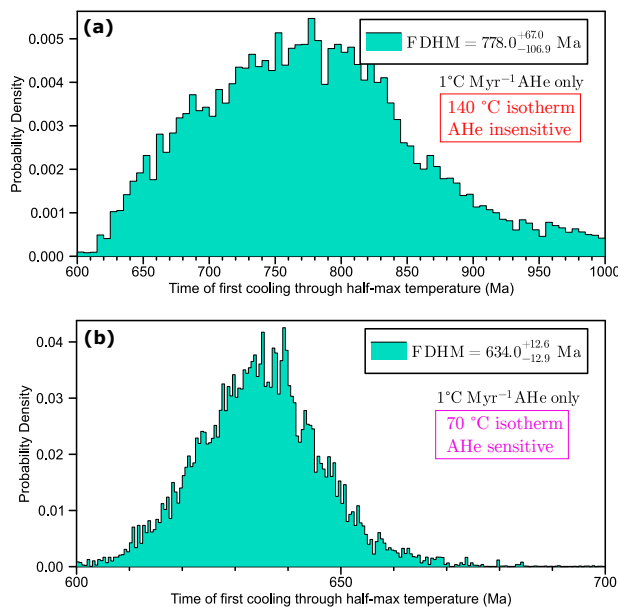
Figure 5. The FDHMs for the AHe-only model shown in Figure 4 for the 1 °C Myr^{-1} cooling rate. (a) FDHM at the actual half-maximum 140 °C isotherm is 778.0 $^{+67.0}_{-106.9}$ Ma, which is highly uncertain and overestimates the time of cooling (yet still contains the true time; note the time of peak cooling for the "true" path is 700 Ma for the total 200 °C of cooling). Note that due to AHe insensitivity, this "cooling time" is entirely controlled by the overall behavior of model paths. Adding a high-temperature constraint makes this pattern worse and the FDHM more inaccurate. (b) FDHM at the 70 °C isotherm is 634.0 $^{+12.6}_{-12.9}$ Ma, which better reflects the sensitivity of the AHe method. This can be visualized in Figure 4 at the intersection between the true path that generated the synthetic data (dashed black curve), the ML path (red curve) from the AHe-only inversion, and the highest QTQt path density. The time window examined for each FDHM estimate was 600–1000 Myr at the 140 °C isotherm and 600–700 Myr at the 70 °C isotherm. Linear interpolation step was 0.1 Myr for the temporal distributions with a histogram bin size of 4 Myr.

Myr^{-1} cooling history are ca. 688 Ma (eU = 10 ppm), 673 Ma (eU = 25 ppm), and 685 Ma (eU = 50 ppm; the oldest closure ages correspond to the largest/high-eU grains). These times are all after the true time of peak cooling at 700 Ma. Thus, AHe dates in isolation cannot constrain the true timing of cooling from temperatures greater than the maximum sensitivity of the (U–Th)/He system, since the apatites are only sensitive to temperatures < 100 °C, and more realistically nearer to < 80 to 40 °C (Figure 4).

This result emphasizes proper assessment of thermochronometric sensitivity with respect to features of a thermal history model, especially the time of initial cooling. The ability to discern model resolution from the output t–T path density is a powerful and useful feature of QTQt (or Bayesian models in general; e.g., Figures 2, 6, and 8). If cooling were slower over a longer interval and/or if reheating were to occur later in the history, then t–T resolution would be further diminished with respect to the initial cooling episode in the Neoproterozoic (McDannell and Keller, 2022, for discussion). In Figure 4, the

intersection between the highest path density, the 70 °C isotherm, and the ML path suggest this is the region where model sensitivity is the highest along the cooling segment (i.e., collapse of the t–T cooling envelope). Rather than fully interpret the cooling signal exhibited in such an inversion (Figure 4), it would be more appropriate to state that cooling through 70 °C (i.e.,

245   maximized AHe sensitivity) occurred at 634.0 $^{+12.6}_{-12.9}$ Ma (Figure 5b).

4   Testing the FDHM method using real data

We also tested the FDHM method on real thermochronological data and inversions from two endmember settings: one from a young pluton in the Swiss Alps with a well characterized late Cenozoic cooling history (Mahéo et al., 2013), and the other from a cratonic setting with a complex thermal history involving multiple heating and cooling events spanning more than two

250   billion years (McDannell and Keller, 2022).

4.1   Bergell pluton, Swiss Alps

We applied the FDHM method to the Bergell pluton since this location is well dated and characterized by a fairly simple Neogene exhumation history (Mahéo et al., 2013; Fox et al., 2014b). Cooling and exhumation of the Bergell pluton was most recently constrained by Mahéo et al. (2013) incorporating multiple thermochronological techniques. Their history interpretation

255   involved three phases: (i) pluton emplacement between ca. 32–28 Ma with rapid initial exhumation from $>$ 25–20 Ma to ca. 17 Ma, and slowed cooling until ca. 10 Ma; (ii) a quiescent phase from ca. 10 to ca. 6–5 Ma; and (iii) an apparent increase in cooling after 6–5 Ma. The accelerated late cooling event is found throughout the Alps (e.g., Valla et al., 2011) and has been attributed to either Messinian base level fall at about 6 Ma, onset of increased climate variability between 5–3 Ma, or intensified alpine glacial erosion at $\leq$ 0.9 Ma (Mahéo et al., 2013, for details). Using thermochronometry coupled with a

260   landscape evolution model, Fox et al. (2014b) further refined the onset of accelerated cooling to 4.5–3.5 Ma and attributed it to enhanced rock uplift and glacial erosion. We applied the FDHM method to quantify the timing of peak cooling for this late event that should hypothetically occur after 5 Ma.

Ketcham et al. (2018) published AFT and AHe data collected from twelve laboratory groups that performed blind dating to compare both the interlab analytical data variation and the submitted thermal history models for two locations, one of which

265   was the Bergell massif in the Swiss Alps (their Sample 2; S2). They presented inverse t–T models for the Bergell, but there is not a published high quality QTQt inversion, so we modeled the Bergell AFT and AHe data here. We remodeled the Lab 5 Analyst 1 and 2 (L5 A1/A2) fission-track datasets for S2 in QTQt from Ketcham et al. (2018), since those data were internally consistent and aligned with the laboratory group median for AFT central age and mean track length. The AFT central ages were ca. 18 Ma with c-axis projected MTLs of $\sim$ 13–14 μm (refer to Appendix A for details). We also incorporated AHe dates

270   generated by Lab 11. They provided six (U-Th)/He single-grain analyses with consistent results and additional contextual information (Ketcham et al., 2018). The Lab 11 mean Ft-corrected AHe date was 6.45 $\pm$ 0.10 Ma, similar to the overall mean AHe date of 6.4 Ma reported in Ketcham et al. (2018) and the original Bergell study of Mahéo et al. (2013) where multi-grain aliquots were analysed.
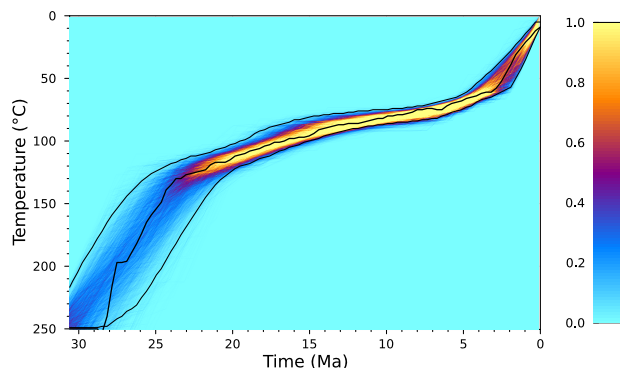
Figure 6. QTQt inversion of Bergell pluton AFT and AHe samples from Labs 5 and 11 from the Ketcham et al. (2018) interlaboratory study. The plot legend is the same as the other QTQt examples discussed previously. The Maximum Mode model ± 95% credible interval from QTQt is also shown (black lines; see text for discussion). Predicted thermochronometer data mostly reproduced all input ages for all representative QTQt paths (i.e., max. likelihood/posterior/mode/expected; Gallagher and Ketcham, 2020).
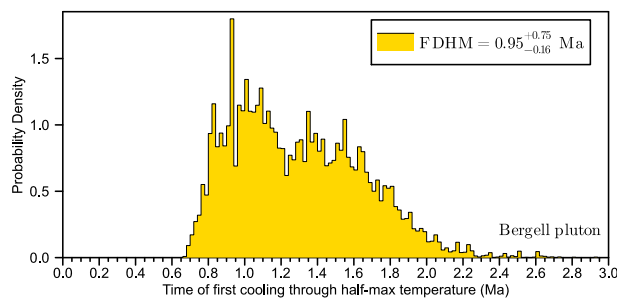
Figure 7. Probability density plot of the FDHM for the Bergell pluton. The time of peak cooling through 30 °C was estimated as $0.95 \,^{+0.75}_{-0.16}$ Ma. The time window examined was between 3.0–0.0 Myr and linear interpolation step was 0.01 Myr for the temporal distributions with a histogram bin size of 0.1 Myr.

The QTQt model general prior was set to 16 ± 16 Myr and 125 ± 125 °C with a present day surface temperature of $5 \pm$
275 5 °C, and a maximum allowed $\delta T/\delta t$ of 30 °C Myr^{-1}. Reheating was prevented and paths were required to begin at 250 °C at 28 ± 4 Ma—to some extent similar to the summary models in Figure 12 of Ketcham et al. (2018). The AFT data were inverted using the Ketcham et al. (2007) annealing model and the D_{par} kinetic parameter (mean etch-figure diameter parallel to the crystallographic c-axis; Donelick et al., 2005) was resampled within the 1σ uncertainty for each sample. The AHe ages range from ca. 5.8–5.1 Ma (Ft-corrected), with an outlier age of 6.9 Ma that was modeled but ignored in the inversion during
280 estimation of the posterior. We also only modeled the five apatite grains that had two crystal terminations.

The QTQt inversion for the Bergell pluton is shown in Figure 6. Our thermal history model agrees with the interpreted three periods of cooling (i.e., fast-slow-fast) outlined in Mahéo et al. (2013), although we maintain that cooling is relatively constant with little variability from ca. 24 Ma to 4 Ma. We overlaid the Maximum Mode (MM) model from QTQt to guide the eye to the last cooling episode in the Bergell history. Where the thermal history is well resolved, the MM gives us a sense of where

285 changes occur in the overall ensemble of t–T paths. The MM is obtained from the distribution of all models sampled. The mode is the peak of a probability distribution in one dimension, whereas in QTQt the t–T space is divided into pixels with a resolution of 1 Myr and 1 °C, where the MM model is the temperature value at each 1 Myr step that has the greatest number of paths passing through it (Gallagher, 2012; Gallagher and Ketcham, 2020). The turning point in the MM model is considered here as an interpretive tool and should be assessed cautiously since the mode may change in any given inversion under different

290 modeling conditions. The MM turning point for the last cooling event is at ca. 3–2 Ma and $\sim$ 60 °C, but could generally occur at any time between ca. 5–2 Ma when examining the individual t–T paths. The important detail is that regardless of the timing of accelerated cooling, the temperature at which cooling begins is stable at 60 °C.

The FDHM for the Bergell pluton is 0.95 $^{+0.75}_{-0.16}$ Ma at the 30 °C isotherm (Figure 7), which generally aligns with the assessment that peak cooling occurred during alpine glaciation near 0.89 Ma. The caveat being that the AHe data require

295 elevated temperatures within the He partial retention zone ($\sim$ 90–40 °C) late in the thermal history to set the young AHe cooling ages, but the resolving power of the AHe data are limited below 50–40 °C. There is also undoubtedly some influence on the final cooling event due to the present day surface temperature boundary condition. Nonetheless, the FDHM result is interesting in that it aligns with a hypothesis for the cause of accelerated erosion due to glaciation in the Alps.

4.2 Hearne craton, SW Hudson Bay margin, Canada

300 The second example presented here is from data collected and modeled from the Hearne craton. The Hearne craton lies at the center of the Canadian Shield and has a cooling history spanning more than 2500 Myr. McDannell and Keller (2022) modeled ZHe, AFT, and AHe data from two combined samples, 97-10-481 and 97-10-499, collected from crystalline basement along the southwestern Hudson Bay margin (Figure 8). The main features of this thermal history are that there is a lack of t–T resolution prior to ca. 1 Ga due to lack of data sensitivity from thermal resetting near that time. Cooling in the Neoproterozoic

305 was followed by an episodic cooling-heating history (Figure 8). The integrated datasets require rapid cooling from $\sim$ 200 °C near 700 Ma to near-surface temperature by $>$ 600 Ma. The subsequent dual thermal peaks (i.e., late Paleozoic and late Mesozoic-early Cenozoic) and intervening periods at low temperatures reproduce a well established Phanerozoic burial and erosion trend that has been recognized across the continental interior of northern Laurentia (e.g., Crowley, 1991; Osadetz et al., 2002; Lorencak et al., 2004; Ault et al., 2009; Feinstein et al., 2009; McDannell et al., 2019, 2022c,d).

310 The Hearne craton FDHM is 669.5 $^{+8.9}_{-5.4}$ Ma at the 100 °C isotherm. The interpreted timing of the cooling peak between ca. 679–665 Ma was associated with deep erosion ($>$ 3 km) during Snowball Earth glaciations in the Cryogenian (McDannell and Keller, 2022). This t–T signal broadly agrees with other high-quality thermochronometric inversions across interior North America (McDannell et al., 2022a) and is discussed in more detail in McDannell and Keller (2022).
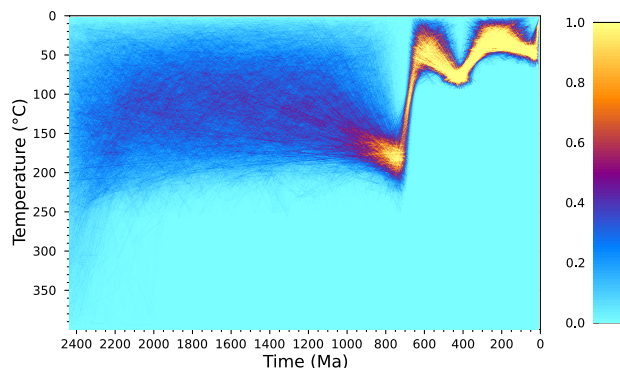
Figure 8. QTQt inversion of ZHe, AFT, and AHe data from the Hearne craton, Canada; plot modified from McDannell and Keller (2022). The interval of interest for the FDHM method is cooling from ~ 200 °C during the Neoproterozoic. Refer to McDannell and Keller (2022) for complete modeling details and for model fits to the observed data.
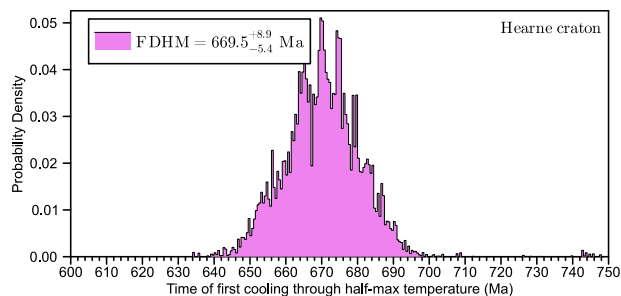
Figure 9. Hearne craton probability density plots of the times at which t–T paths crossed the approximate half-maximum 100 °C isotherm. FDHM is 669.5 $^{+8.9}_{-5.4}$ Ma. The time window examined was between 750–600 Myr and the interpolation step was 0.1 Myr for the plotted distribution with a histogram bin size of 1 Myr. FDHM shown here differs slightly from the FDHM (i.e., 668.5 $^{+10.1}_{-6.2}$ Ma) discussed in McDannell and Keller (2022) due to a narrower time window and a smaller interpolation step in this work.

5 Average time of peak cooling from multiple FDHMs

An average peak cooling time may be desired and is included as an option in the Julia script on *OpenThermochronology*. It may be practical to consolidate the FDHMs from multiple t–T inversions for samples within a study area that share a common thermal history. We can select the temporal distributions from different FDHMs, which in most cases will be characterized by asymmetric errors that cannot be combined in quadrature but can be combined using a Monte Carlo method. The distributions often constitute arrays of different length, therefore we sample randomly from the individual distributions (i.e., randomly select 20,000 samples from each posterior distribution) to generate arrays of the same length and calculate a weighted mean

distribution (with symmetric errors) of all the FDHMs being considered. A normalized probability density of the new random distribution is then plotted as a histogram, similar to the plots shown previously (e.g., Figure 9).

6 Summary of the FDHM method

This study introduces and validates a novel approach for approximating the peak timing of cooling in inverse models of
325 thermochronological data. This method, known as the Full time-Distribution at Half-Maximum temperature (FDHM), provides a quantitative technique to systematically analyze thermal history model output. It is particularly effective for smooth thermal histories with a single inflection point that are well-resolved in time-temperature space, especially those incorporating data from multiple thermochronometers. However, caution is advised when applying the FDHM method to single-thermochronometer inversions due to time-temperature resolution limitations. In such cases, interpretations should be made with consideration of
330 the mineral's effective temperature sensitivity.

Code availability. The FDHM code is written in the Julia language and can be found at: https://github.com/OpenThermochronology

Data availability. All QTQt model setup information and outputs for previously unpublished examples presented herein are available upon request.

Appendix A: Modeling details

335 *Bergell pluton.* The L5 AFT data were generated using the external detector method and a 5.5 M acid etch; all other information about those results can be found in Ketcham et al. (2018). The L5 A1 AFT central age is 18.4 ± 1.0 Ma (n = 20; p(χ^2) = 0.36) with a conventional MTL of 13.1 ± 1.8 μm (n = 100) and c-axis projected MTL of 14.3 ± 1.2 μm. The L5 A2 AFT central age is 18.2 ± 1.3 Ma (n = 20; p(χ^2) = 0.95) with a conventional MTL of 12.3 ± 1.6 μm (n = 105) and c-axis projected MTL = 13.7 ± 1.5 μm. An outlier of the L5 dataset was the measured D_{par} values of 3.07 ± 0.44 μm (A1) and 2.97 ± 0.63 μm (A2), which
340 were larger than the D_{par} measurements from the other labs whose mean was closer to $\sim$ 1.85–1.9 μm. QTQt temperature step(s) for diffusion and radiation damage = 1. Note that it is still possible for the D_{par} values to be sampled outside of the measured range if the QTQt MCMC search finds better fits to the observed data. For reference, the Bergell max. likelihood (best-fit) model path in QTQt required a predicted D_{par} of $\sim$ 2.92 μm (observed: 3.07 μm; sampled: 3.015 ± 0.23 μm) for A1 AFT data and a predicted D_{par} of $\sim$ 2.29 μm (observed: 2.97 μm; sampled: 2.45 ± 0.129 μm) for A2 AFT data.

345 *Author contributions.* Contributor Roles Taxonomy (CRediT). McDannell: conceptualization, methodology, investigation, formal analysis, software, visualization, writing–original draft/review/editing, funding acquisition. Keller: software, conceptualization, funding acquisition, methodology, writing–review/editing.

Competing interests. C.B. Keller is an associate editor of the journal Geochronology and the authors have no other competing interests to declare.

350 *Acknowledgements.* Thanks to Matt Fox (UCL) for valuable discussion. This work was supported by NSF EAR-SGP award 2044800 to C.B.K. and K.T.M.

References

Ault, A. K., Flowers, R. M., and Bowring, S. A.: Phanerozoic burial and unroofing history of the western Slave craton and Wopmay orogen from apatite (U-Th)/He thermochronometry, Earth and Planetary Science Letters, 284, 1–11, https://doi.org/10.1016/j.epsl.2009.02.035, https://linkinghub.elsevier.com/retrieve/pii/S0012821X09001356, 2009.

Braun, J.: Quantitative constraints on the rate of landform evolution derived from low-temperature thermochronology, in: Reviews in Mineralogy and Geochemistry, edited by Reiners, P. W. and Ehlers, T. A., vol. 58, pp. 351–374, Mineralogical Society of America and Geochemical Society, Washington, DC, United States (USA), 2005.

Braun, J., van der Beek, P., Valla, P., Robert, X., Herman, F., Glotzbach, C., Pedersen, V., Perry, C., Simon-Labric, T., and Prigent, C.: Quantifying rates of landscape evolution and tectonic processes by thermochronology and numerical modeling of crustal heat transport using PECUBE, Tectonophysics, 524-525, 1–28, https://doi.org/10.1016/j.tecto.2011.12.035, 2012.

Carlson, W. D., Donelick, R. A., and Ketcham, R. A.: Variability of apatite fission-track annealing kinetics: I. Experimental results, American Mineralogist, 84, 1213–1223, https://doi.org/10.2138/am-1999-0901, 1999.

Crowley, K. D.: Thermal history of Michigan Basin and Southern Canadian Shield from apatite fission track analysis, Journal of Geophysical Research, 96, 697–711, https://doi.org/10.1029/90JB02174, http://doi.wiley.com/10.1029/90JB02174, 1991.

Dodson, M. H.: Closure temperature in cooling geochronological and petrological systems, Contributions to Mineralogy and Petrology, 40, 259–274, https://doi.org/10.1007/BF00373790, 1973.

Donelick, R. A., O'Sullivan, P. B., and Ketcham, R. A.: Apatite Fission-Track Analysis, Reviews in Mineralogy and Geochemistry, 58, 49–94, https://doi.org/10.2138/rmg.2005.58.3, 2005.

Ehlers, T. A. and Farley, K. A.: Apatite (U-Th)/He thermochronometry: Methods and applications to problems in tectonic and surface processes, Earth and Planetary Science Letters, 206, 1–14, https://doi.org/10.1016/S0012-821X(02)01069-5, 2003.

Feinstein, S., Kohn, B., Osadetz, K., Everitt, R., and O'Sullivan, P.: Variable Phanerozoic thermal history in the Southern Canadian Shield: Evidence from an apatite fission track profile at the Underground Research Laboratory (URL), Manitoba, Tectonophysics, 475, 190–199, https://doi.org/10.1016/j.tecto.2009.01.016, 2009.

Flowers, R. M., Ketcham, R. A., Shuster, D. L., and Farley, K. A.: Apatite (U–Th)/He thermochronometry using a radiation damage accumulation and annealing model, Geochimica et Cosmochimica Acta, 73, 2347–2365, https://doi.org/10.1016/j.gca.2009.01.015, https://linkinghub.elsevier.com/retrieve/pii/S001670370900043X, 2009.

Flowers, R. M., Ketcham, R. A., Enkelmann, E., Gautheron, C., Reiners, P. W., Metcalf, J. R., Danišík, M., Stockli, D. F., and Brown, R. W.: (U-Th)/He chronology: Part 2. Considerations for evaluating, integrating, and interpreting conventional individual aliquot data, Bulletin of the Geological Society of America, 135, 137–161, https://doi.org/10.1130/B36268.1, https://doi.org/10.1130/B36268.1, 2023.

Fox, M. and Carter, A.: Heated Topics in Thermochronology and Paths towards Resolution, Geosciences, 10, 375, https://doi.org/10.3390/geosciences10090375, https://www.mdpi.com/2076-3263/10/9/375, 2020.

Fox, M. and Shuster, D. L.: The influence of burial heating on the (U-Th)/He system in apatite: Grand Canyon case study, Earth and Planetary Science Letters, 397, 174–183, https://doi.org/10.1016/j.epsl.2014.04.041, 2014.

Fox, M. and Shuster, D. L.: Lazed and Diffused: Untangling Noble Gas Thermochronometry Data for Exhumation Rates, Elements, 16, 337–342, https://doi.org/10.2138/gselements.16.5.337, https://pubs.geoscienceworld.org/msa/elements/article/16/5/337/592246/Lazed-and-Diffused-Untangling-Noble-Gas, 2020.

Fox, M., Herman, F., Willett, S. D., and May, D. A.: A linear inversion method to infer exhumation rates in space and time from thermochronometric data, Earth Surface Dynamics, 2, 47–65, https://doi.org/10.5194/esurf-2-47-2014, 2014a.

390   Fox, M., Reverman, R., Herman, F., Fellin, M. G., Sternai, P., and Willett, S. D.: Rock uplift and erosion rate history of the Bergell intrusion from the inversion of low temperature thermochronometric data, Geochemistry, Geophysics, Geosystems, 15, 1235–1257, 2014b.

Fox, M., Tripathy-Lang, A., Shuster, D. L., Winn, C., Karlstrom, K., and Kelley, S.: Westernmost Grand Canyon incision: Testing thermochronometric resolution, Earth and Planetary Science Letters, 474, 248–256, https://doi.org/https://doi.org/10.1016/j.epsl.2017.06.049, https://www.sciencedirect.com/science/article/pii/S0012821X17303734, 2017.

395   Galbraith, R. F.: Statistics for Fission Track Analysis, Chapman and Hall/CRC, New York, NY, https://doi.org/10.1201/9781420034929, https://www.taylorfrancis.com/books/9781420034929, 2005.

Gallagher, K.: Evolving temperature histories from apatite fission-track data, Earth and Planetary Science Letters, 136, 421–435, https://doi.org/10.1016/0012-821X(95)00197-K, https://linkinghub.elsevier.com/retrieve/pii/0012821X9500197K, 1995.

Gallagher, K.: Transdimensional inverse thermal history modeling for quantitative thermochronology, Journal of Geophysical Research:
400   Solid Earth, 117, https://doi.org/10.1029/2011JB008825, 2012.

Gallagher, K.: Trans-Dimensional Markov Chain Monte Carlo Methods Applied to Geochronology and Thermochronology, in: Applications of Data Assimilation and Inverse Problems in the Earth Sciences, edited by Ismail-Zadeh, A., Jones, D., Castelli, F., and Sanchez, S., Special Publications of the International Union of Geodesy and Geophysics, pp. 175–195, Cambridge University Press, Cambridge, https://doi.org/10.1017/9781009180412.012, 2023.

405   Gallagher, K. and Ketcham, R. A.: Comment on the reply to the Comment on "Thermal history modelling: HeFTy vs. QTQt" by Vermeesch and Tian, Earth-Science Reviews (2014), 139, 279–290, Earth-Science Reviews, 203, 102 878, https://doi.org/10.1016/j.earscirev.2019.102878, https://linkinghub.elsevier.com/retrieve/pii/S0012825218301259, 2020.

Gautheron, C. and Zeitler, P. K.: Noble gases deliver cool dates from hot rocks, Elements, 16, 303–309, https://doi.org/10.2138/GSELEMENTS.16.5.303, 2020.

410   Gautheron, C., Tassan-Got, L., Barbarand, J., and Pagel, M.: Effect of alpha-damage annealing on apatite (U-Th)/He thermochronology, Chemical Geology, 266, 157–170, https://doi.org/10.1016/j.chemgeo.2009.06.001, 2009.

Ginster, U., Reiners, P. W., Nasdala, L., and Chanmuang, C.: Annealing kinetics of radiation damage in zircon, Geochimica et Cosmochimica Acta, 249, 225–246, https://doi.org/10.1016/j.gca.2019.01.033, 2019.

Green, P. F. and Duddy, I. R.: Thermal History Reconstruction in Sedimentary Basins using Apatite Fission-Track Analysis and Related
415   Techniques, in: Analyzing the Thermal History of Sedimentary Basins: Methods and Case Studies, pp. 65–104, Society for Sedimentary Geology, https://doi.org/10.2110/sepmsp.103.065, 2012.

Guenthner, W. R.: Implementation of an Alpha Damage Annealing Model for Zircon (U-Th)/He Thermochronology With Comparison to a Zircon Fission Track Annealing Model, Geochemistry, Geophysics, Geosystems, 22, https://doi.org/10.1029/2019GC008757, 2021.

Guenthner, W. R., Reiners, P. W., Ketcham, R. A., Nasdala, L., and Giester, G.: Helium diffusion in natural zircon: radiation
420   damage, anisotropy, and the interpretation of zircon (U-Th)/He thermochronology, American Journal of Science, 313, 145–198, https://doi.org/10.2475/03.2013.01, http://www.ajsonline.org/content/313/3/145.abstract, 2013.

Harrison, T. M., Armstrong, R. L., Naeser, C. W., and Harakal, J. E.: Geochronology and thermal history of the Coast Plutonic Complex, near Prince Rupert, British Columbia, Canadian Journal of Earth Sciences, 16, 400–410, https://doi.org/10.1139/e79-038, https://doi.org/10.1139/e79-038, 1979.

425   Herman, F., Copeland, P., Avouac, J. P., Bollinger, L., Maheo, G., Le Fort, P., Rai, S., Foster, D., Pecher, A., Stuwe, K., and Henry, P.: Exhumation, crustal deformation, and thermal structure of the Nepal Himalaya derived from the inversion of thermochronological and thermobarometric data and modeling of the topography, Journal of Geophysical Research: Solid Earth, 115, https://doi.org/10.1029/2008JB006126, 2010.

House, M. A., Wernicke, B. P., and Farley, K. A.: Dating topography of the Sierra Nevada, California, using apatite (U- Th)/He ages, Nature,
430   396, 66–69, https://doi.org/10.1038/23926, http://dx.doi.org/10.1038/23926, 1998.

Issler, D. R.: An inverse model for extracting thermal histories from apatite fission track data: instructions and software for the Windows 95 environment, Tech. rep., Geological Survey of Canada, Open File Report 2325, https://doi.org/10.4095/208313, https://doi.org/10.4095/208313, 1996a.

Issler, D. R.: Optimizing time step size for apatite fission track annealing models, Computers and Geosciences, 22, 67–74,
435   https://doi.org/10.1016/0098-3004(95)00057-7, 1996b.

Issler, D. R., McDannell, K. T., O'Sullivan, P. B., and Lane, L. S.: Simulating sedimentary burial cycles – Part 2: Elemental-based multikinetic apatite fission-track interpretation and modelling techniques illustrated using examples from northern Yukon, Geochronology, 4, 373–397, https://doi.org/10.5194/gchron-4-373-2022, 2022.

Keller, C. B., McDannell, K. T., Guenthner, W., and Shuster, D. L.: Thermochron.jl: Open-source time-Temperature inversion of ther-
440   mochronometric data, https://doi.org/10.17605/OSF.IO/WQ2U5, 2022.

Ketcham, R. A.: Forward and Inverse Modeling of Low-Temperature Thermochronometry Data, Reviews in Mineralogy and Geochemistry, 58, 275–314, https://doi.org/10.2138/rmg.2005.58.11, https://pubs.geoscienceworld.org/rimg/article/58/1/275-314/87556, 2005.

Ketcham, R. A., Donelick, R. A., and Carlson, W. D.: Variability of apatite fission-track annealing kinetics: III. Extrapolation to geological time scales, American Mineralogist, 84, 1235–1255, https://doi.org/10.2138/am-1999-0903, 1999.

445   Ketcham, R. A., Carter, A., Donelick, R. A., Barbarand, J., and Hurford, A. J.: Improved modeling of fission-track annealing in apatite, American Mineralogist, 92, 799–810, https://doi.org/10.2138/am.2007.2281, 2007.

Ketcham, R. A., Donelick, R. A., Balestrieri, M. L., and Zattin, M.: Reproducibility of apatite fission-track length data and thermal history reconstruction, Earth and Planetary Science Letters, 284, 504–515, https://doi.org/10.1016/j.epsl.2009.05.015, 2009.

Ketcham, R. A., van der Beek, P., Barbarand, J., Bernet, M., and Gautheron, C.: Reproducibility of Thermal History
450   Reconstruction From Apatite Fission-Track and (U-Th)/He Data, Geochemistry, Geophysics, Geosystems, 19, 2411–2436, https://doi.org/10.1029/2018GC007555, 2018.

Kohn, B. P., Gleadow, A. J. W., Brown, R. W., Gallagher, K., Lorencak, M., and Noble, W. P.: Visualizing thermotectonic and denudation histories using apatite fission track thermochronology, in: Reviews in Mineralogy and Geochemistry, edited by Reiners, P. W. and Ehlers, T. A., vol. 58, pp. 527–565, Mineralogical Society of America and Geochemical Society, Washington, DC, United States (USA),
455   https://doi.org/10.2138/rmg.2005.58.20, 2005.

Lorencak, M., Kohn, B., Osadetz, K., and Gleadow, A.: Combined apatite fission track and (U–Th)/He thermochronometry in a slowly cooled terrane: results from a 3440-m-deep drill hole in the southern Canadian Shield, Earth and Planetary Science Letters, 227, 87–104, https://doi.org/10.1016/j.epsl.2004.08.015, https://linkinghub.elsevier.com/retrieve/pii/S0012821X04005060, 2004.

Mahéo, G., Gautheron, C., Leloup, P. H., Fox, M., Tassant-Got, L., and Douville, E.: Neogene exhumation history of the Bergell massif
460   (southeast Central Alps), Terra Nova, 25, 110–118, https://doi.org/10.1111/ter.12013, 2013.

Markevich, N. and Gertner, I.: Comparison among methods for calculating FWHM, Nuclear Instruments and Methods in Physics Research Section A: Accelerators, Spectrometers, Detectors and Associated Equipment, 283, 72–77, https://doi.org/10.1016/0168-9002(89)91258-8, https://linkinghub.elsevier.com/retrieve/pii/0168900289912588, 1989.

Mattinson, J. M.: Age, origin, and thermal histories of some plutonic rocks from the Salinian block of California, Contributions to Mineralogy and Petrology, 67, 233–245, https://doi.org/10.1007/BF00381451, 1978.

McDannell, K. T.: Notes on statistical age dispersion in fission-track datasets: the chi-square test, annealing variability, and analytical considerations, EarthArXiv, pp. 1–4, https://doi.org/10.31223/OSF.IO/UJ4HX, 2020.

McDannell, K. T. and Flowers, R. M.: Vestiges of the ancient: Deep-time noble gas thermochronology, Elements, 16, 325–330, https://doi.org/10.2138/GSELEMENTS.16.5.325, 2020.

McDannell, K. T. and Issler, D. R.: Simulating sedimentary burial cycles – Part 1: Investigating the role of apatite fission track annealing kinetics using synthetic data, Geochronology, 3, 321–335, https://doi.org/10.5194/gchron-3-321-2021, 2021.

McDannell, K. T. and Keller, C. B.: Cryogenian glacial erosion of the central Canadian Shield: The "late" Great Unconformity on thin ice, Geology, 50, 1336–1340, https://doi.org/10.1130/G50315.1, https://pubs.geoscienceworld.org/geology/article/50/12/1336/616595/Cryogenian-glacial-erosion-of-the-central-Canadian, 2022.

McDannell, K. T., Schneider, D. A., Zeitler, P. K., O'Sullivan, P. B., and Issler, D. R.: Reconstructing deep-time histories from integrated thermochronology: An example from southern Baffin Island, Canada, Terra Nova, 31, 189–204, https://doi.org/10.1111/ter.12386, 2019.

McDannell, K. T., Keller, C. B., Guenthner, W. R., Zeitler, P. K., and Shuster, D. L.: Thermochronologic constraints on the origin of the Great Unconformity, Proceedings of the National Academy of Sciences, 119, e2118682 119, https://doi.org/10.1073/pnas.2118682119, 2022a.

McDannell, K. T., Keller, C. B., Guenthner, W. R., Zeitler, P. K., and Shuster, D. L.: Reply to Flowers et al.: Existing thermochronologic data constrain Snowball glacial erosion below the Great Unconformity, Proceedings of the National Academy of Sciences, 119, e2209946 119, https://doi.org/10.1073/pnas.2209946119, 2022b.

McDannell, K. T., O'Sullivan, P. B., Gallagher, K., and Boroughs, S.: Phanerozoic sedimentary cover history of the Hudson Platform: a heuristic modeling perspective, EarthArXiv, pp. 1–47, https://doi.org/10.31223/X5M05W, 2022c.

McDannell, K. T., Pinet, N., and Issler, D. R.: Exhuming the Canadian Shield: preliminary interpretations from low-temperature thermochronology and significance for the sedimentary succession of the Hudson Bay Basin, in: Sedimentary basins of northern Canada: contributions to a 1000 Ma geological journey and insight on resource potential, edited by Lavoie, D. and Dewing, K., pp. 287–322, Geological Survey of Canada, Bulletin 609, https://doi.org/10.4095/326100, 2022d.

Osadetz, K., Kohn, B., Feinstein, S., and O'Sullivan, P.: Thermal history of Canadian Williston basin from apatite fission-track thermochronology—implications for petroleum systems and geodynamic history, Tectonophysics, 349, 221–249, https://doi.org/10.1016/S0040-1951(02)00055-0, https://linkinghub.elsevier.com/retrieve/pii/S0040195102000550, 2002.

Reiners, P. W. and Brandon, M. T.: Using thermochronology to understand orogenic erosion, Annual Review of Earth and Planetary Sciences, 34, 419–466, https://doi.org/10.1146/annurev.earth.34.031405.125202, 2006.

Reiners, P. W., Carlson, R. W., Renne, P. R., Cooper, K. M., Granger, D. E., McLean, N. M., and Schoene, B.: Geochronology and Thermochronology, John Wiley & Sons, https://doi.org/10.1002/9781118455876, 2017.

Shuster, D. L., Flowers, R. M., and Farley, K. A.: The influence of natural radiation damage on helium diffusion kinetics in apatite, Earth and Planetary Science Letters, 249, 148–161, https://doi.org/10.1016/j.epsl.2006.07.028, 2006.

Stephenson, J., Gallagher, K., and Holmes, C.: A Bayesian approach to calibrating apatite fission track annealing models for laboratory and geological timescales, Geochimica et Cosmochimica Acta, 70, 5183–5200, https://doi.org/10.1016/j.gca.2006.07.027, 2006.

Stüwe, K., White, L., and Brown, R.: The influence of eroding topography on steady-state isotherms. Application to fission track analysis, Earth and Planetary Science Letters, 124, 63–74, 1994.

Valla, P. G., Shuster, D. L., and Van Der Beek, P. A.: Significant increase in relief of the European Alps during mid-Pleistocene glaciations, Nature Geoscience, 4, 688–692, https://doi.org/10.1038/ngeo1242, 2011.

Vermeesch, P.: Statistics for Fission-Track Thermochronology, in: Fission-Track Thermochronology and its Application to Geology, edited by Malusa, M. G. and Fitzgerald, P., chap. 6, pp. 109–122, Springer International Publishing, New York, 1 edn., https://doi.org/10.1007/978-3-319-89421-8_6, 2019.

Vermeesch, P.: Maximum depositional age estimation revisited, Geoscience Frontiers, 12, 843–850, https://doi.org/10.1016/j.gsf.2020.08.008, 2021.

Vermeesch, P. and Tian, Y.: Thermal history modelling: HeFTy vs. QTQt, Earth-Science Reviews, 139, 279–290, https://doi.org/10.1016/j.earscirev.2014.09.010, 2014.

Whipp, D. M., Kellett, D. A., Coutand, I., and Ketcham, R. A.: Short communication: Modeling competing effects of cooling rate, grain size, and radiation damage in low-temperature thermochronometers, Geochronology, 4, 143–152, https://doi.org/10.5194/gchron-4-143-2022, https://gchron.copernicus.org/articles/4/143/2022/, 2022.

Willett, C. D., Fox, M., and Shuster, D. L.: A helium-based model for the effects of radiation damage annealing on helium diffusion kinetics in apatite, Earth and Planetary Science Letters, 477, 195–204, https://doi.org/10.1016/j.epsl.2017.07.047, 2017.

Willett, S. D.: Inverse modeling of annealing of fission tracks in apatite 1: A controlled random search method, American Journal of Science, 297, 939–969, https://doi.org/10.2475/ajs.297.10.939, 1997.

Zeitler, P. K., Meltzer, A. S., Brown, L., Kidd, W. S., Lim, C., and Enkelmann, E.: Tectonics and topographic evolution of Namche Barwa and the easternmost Lhasa block, Tibet, in: Toward an Improved Understanding of Uplift Mechanisms and the Elevation History of the Tibetan Plateau, vol. 507, pp. 23–58, Geological Society of America, https://doi.org/10.1130/2014.2507(02), https://pubs.geoscienceworld.org/books/book/669/chapter/3807575, 2014.